Atmos. Chem. Phys. Discuss., 13, 27287–27326, 2013
www.atmos-chem-phys-discuss.net/13/27287/2013/
doi:10.5194/acpd-13-27287-2013

Atmospheric Chemistry and Physics Discussions

In-situ measurement of atmospheric CO_2 at the four WMO/GAW stations in China

S. X Fang[1], L. X. Zhou[1], P. P. Tans[2], P. Ciais[3], M. Steinbacher[4], L. Xu[1], and T. Luan[1]

[1]Chinese Academy of Meteorological Sciences (CAMS), China Meteorological Administration (CMA), Beijing, China
[2]Earth System Research Laboratory (ESRL), National Oceanic and Atmospheric Administration (NOAA), Boulder, CO, USA
[3]Laboratory for the Science of Climate and the Environment (LSCE), Paris, France
[4]Empa, Swiss Federal Laboratories for Materials Science and Technology, Laboratory for Air Pollution/Environmental Technology, Duebendorf, Switzerland

Received: 31 August 2013 – Accepted: 14 October 2013 – Published: 21 October 2013

Correspondence to: L. X. Zhou (zhoulx@cams.cma.gov.cn)

Published by Copernicus Publications on behalf of the European Geosciences Union.

Abstract

Atmospheric carbon dioxide (CO_2) mole fractions were continuously measured from January 2009 to December 2011 at 4 atmospheric observatories in China ((Lin'an, LAN), (Longfengshan, LFS), (Shangdianzi, SDZ), and (Waliguan, WLG)) using Cavity Ring Down Spectroscopy instruments. All sites are regional (LAN, LFS, SDZ) or global (WLG) measurement stations of the World Meteorological Organization/Global Atmosphere Watch program (WMO/GAW). LAN is located near the megacity of Shanghai, in China's most economically developed region. LFS is in a forest and rice production area, close to the city of Harbin in the northern east of China. SDZ is located 150 km north east of Beijing. WLG, hosting the longest record of measured CO_2 mole fractions in China, is a high altitude site in northwest China recording background CO_2 values. The CO_2 growth rates are 2.2 ± 0.2 ppm yr^{-1} for LAN, 2.3 ± 0.2 ppm yr^{-1} for LFS, 2.0 ± 0.2 ppm yr^{-1} for SDZ, and 1.2 ± 0.1 ppm yr^{-1} (1σ) for WLG, during the period of 2009 to 2011. The growth rate at WLG may be underestimated due to the data gaps during the observation period. The highest annual mean CO_2 mole fraction of 404.1 ± 4.1 ppm was observed at LAN in 2011. A comprehensive analysis of CO_2 variations, their diurnal and seasonal cycles as well as the analysis of the influence of different wind regimes on the CO_2 mole fractions allows a thorough characterization of the sampling sites and of the key processes driving the CO_2 mole fractions. These data form a basis to improve our understanding of atmospheric CO_2 variations in China and the underlying fluxes, using atmospheric inversion models.

1 Introduction

Carbon dioxide (CO_2) represents the most important contribution to increased radiative forcing (IPCC, 2007). The increase of atmospheric CO_2 of ~ 110 ppm above pre-industrial level has been unequivocally attributed to human emissions (GLOBALVIEW, 2012; Keeling, 1993). These emissions are mainly coming from fossil fuel burning and

ACPD
13, 27287–27326, 2013

land-use changes (Houghton, 2003; Peters et al., 2012). The oceans and terrestrial ecosystems act as sinks for atmospheric CO_2 and absorb approximately half of the anthropogenic emissions (Ballantyne et al., 2012). To enhance our understanding of the carbon cycle, it is crucial to quantify atmospheric CO_2 variations as they are influenced by regional fluxes (Peters et al., 2007; Tans et al., 1990). For this purpose, 55 yr ago, long-term measurements of atmospheric CO_2 concentration began at Mauna Loa, Hawaii (Keeling et al., 1976; Keeling, 2008). So far there are more than 150 sites around the world where greenhouse gas concentrations are measured (Artuso et al., 2009; Dlugokencky et al., 1995; Necki et al., 2003; Sirignano et al., 2010; Tans et al., 1990; WMO, 2012). Studies show that the current global CO_2 observation network can at best constrain emissions at continental scales, and that tropical regions remain unconstrained because observations in that region are too sparse (Chevallier et al., 2011; Thompson et al., 2009). Regional networks with ongoing CO_2 observations measure gradients between stations, which can be used to retrieve information on regional emissions and sinks. At present, relatively dense networks exist over North America and Western Europe, which allow us to constrain regional fluxes using inverse models (e.g. Broquet et al., 2013; Gourdji et al., 2012). But North East Asia, a region of fast economic growth with high emissions, is not adequately sampled, and global inversion results give divergent results for its CO_2 budget (e.g. Peylin et al., 2013; Sirignano et al., 2010).

With the rapid development of its economy, China has become the number one fossil fuel CO_2 emitter in 2006 and emitted 1.8 Pg C in 2011 (Le Quéré et al., 2013; Marland, 2012). Nevertheless, the emissions of China deduced from energy statistics are uncertain, and could be higher than currently reported by up to 0.38 Pg C yr^{-1} (Guan et al., 2012). Peters et al. (2011) also reported that more than half of the growth in global CO_2 emissions from 1990 to 2008 took place in China. However, China is a late starter of atmospheric greenhouse gas observations. In the past years, there were lots of short-term CO_2 measurement campaigns and research programs. Most of them focused on emissions from agricultural sources or urban areas (Fu et al., 2009; Lei and Yang, 2010;

ACPD
13, 27287–27326, 2013

Liu et al., 2009; Tang et al., 2006; Xing et al., 2005). Long-term atmospheric CO_2 observations in China have been relatively sparse. The China Meteorological Administration (CMA) has been responsible for background greenhouse gas measurements. The first station installed in China is Mt. Waliguan (WLG) in the Qinghai province, at 3816 m a.s.l. Since May 1991 CMA has collected weekly air samples in glass flasks. These samples were shipped to the National Oceanic and Atmospheric Administration (NOAA) Earth System Research Laboratory (ESRL) in Boulder, Colorado, United States and analyzed for a suite of greenhouse gases. In 1994, the station was established as a global World Meteorological Organization (WMO)/Global Atmosphere Watch (GAW) measurement site, and was equipped with CO_2 in-situ measurements [LI-COR, nondispersive infrared (NDIR) analyzer]. This instrument produced nearly fourteen years of high quality data, which is the longest continuous atmospheric CO_2 record in China (Zhou et al., 2003, 2005, 2006). In 2009, the aging instrument was replaced by a Cavity Ring Down Spectroscopy (CRDS) analyzer (G1301, Picarro Inc.). Three GHGs continuous measurement stations were established as regional WMO/GAW sites at Lin'an (LAN) in Zhejiang province (near Shanghai), Longfengshan (LFS) in Heilongjiang province (near Harbin, in the Northeast of China), and Shangdianzi (SDZ) near Beijing, respectively. Initially, those were automatic weather stations only, and in-situ CO_2 measurement systems began in 2009 using CRDS instruments (G1301). In this study, we present and analyze the first 3 yr of measurements at the four stations.

2 Experimental

2.1 Sampling sites

Locations of the Lin'an (LAN), Longfengshan (LFS), Shangsianzi (SDZ) and Mt. Waliguan (WLG) are shown in Fig. 1. LAN is located in the center of Yangzi Delta area, China and is about 50 km from Hangzhou (Capital of Zhejiang Province) and 200 km from Shanghai (the largest economic center in China). This station is approximately

ACPD
13, 27287–27326, 2013

6 km northeast of the town of Lin'an, which has a population of ~ 100 000. Lin'an is a tourist town and has no industries with strong CO_2 emissions. North of the LAN station (1.4 km away) is a small factory where charcoal is manufactured from bamboo wood. The station is built on the top of a small hill with pieces of paddy rice field surrounded.

LFS is 140 km southeast of Harbin city. Wuchang, the nearest city, has ~ 200 000 inhabitants and is 40 km to northwest of the site. The station is located on the northwest edge of the Longfengshan water reservoir, which has an area of 20 km^2. The reservoir's dam is located 0.1 km to the north of LFS. Right beyond the dam to the north, there is a small area of paddy rice field and several small villages (100 inhabitants). The station is located in a forest park with mainly pine trees.

SDZ is located at 150 km northeast of Beijing. The observatory is built on a mountain-side (with the highest peak on the north). There is a small village (~ 300 inhabitants) at about 0.8 km the south of the station. A railway used by diesel-driven trains runs from south to north, ~ 0.6 km away from the station. Local vegetation is mainly shrubs and corn.

WLG is situated in western China at 3816 m a.s.l., remotely from industrial and populated centers. Measurements from WLG provide essential information on sources and sinks over the Eurasian continent (Zhou et al., 2004, 2005). At SDZ, LAN and LFS, the sampling inlets were initially fixed on the top of wind poles (10 m above the ground). Near each sampling inlet, a wind direction and speed sensor were also installed. The distance from the wind pole to the nearby observatory buildings are 60, 25 and 65 m for SDZ, LAN, and LFS, respectively, to ensure that the air sample is minimally affected by human activities in the buildings. In 2010, new sampling towers of 50 m and 80 m height were erected at LAN and LFS, respectively. In 2011, an 80 m sampling tower was built at SDZ. A second sampling inlet was installed at the top level of each tower, in addition to the previous 10 m high inlet. The air intake into each Picarro analyzer then switched between the 10 m and the top-level intake every 5 min at the three stations. Because of the short records available from the highest level at the three regional stations, we mainly discuss measurements from the 10 m intake. At WLG station, the

ACPD
13, 27287–27326, 2013

air sample inlet is fixed at an 80 m height of an 89 m sampling tower located 15 m from the laboratory.

2.2 Measurement system

CRDS systems (G1301, Picarro Inc.) are used for continuous measurements of atmospheric CO_2 and CH_4. This type of instrument has been proven suitable for making precise measurement of CO_2 and CH_4 mole fraction since its response is both highly linear and very stable (Chen et al., 2010; Crosson, 2008). The detailed schematic of the measurement setup is described in Fang et al. (2003). The residence time of the air from the top of the inlets to inlet of the Picarro is less than 30 s. The individual systems were installed in 1 January 2009 at LAN, LFS, SDZ, and WLG, respectively, and are still running. In this study, the analysis is restricted to the January 2009 to December 2011 period.

2.3 Calibration, quality control and data processing

Carbon dioxide mole fractions are referenced to a Working High standard (WH) and a Working Low standard (WL). Additionally, a calibrated cylinder filled with compressed ambient air is used as a target gas (T) to check the precision and stability of the system routinely. All standard gases are pressurized in 29.5 L treated aluminum alloy cylinders (Scott-Marrin Inc.) fitted with high-purity, two-stage gas regulators. The standard gases are calibrated with cylinders assigned by the GAW CO_2 Central Calibration Laboratory operated by NOAA/ESRL. All data are reported on the WMO X2007 scale (Zhao and Tans, 2006; Zhao et al., 1997). Calibration of the working standards and target gases is done at CMA's Central Laboratory in Beijing before and after use at the measurement stations. An automated sampling module equipped with a VICI 8 port multi-position valve is designed to sample from separate gas streams (standard gas cylinders and ambient air). The three standards are analyzed by the system for 5 min every 6 h.

ACPD
13, 27287–27326, 2013

The discrete flask samples collected weekly at WLG have been measured by the Carbon Cycle Greenhouse Gases group (CCGG) of NOAA/ESRL in Boulder, CO, USA. Two flask samples were collected in series at 08:00 local time (LT) using glass flasks and a portable battery powered sampling apparatus with a 5 m (a.g.l.) intake height (Dlugokencky et al., 1994). The samples were measured at NOAA using a non-dispersive infrared (NDIR) analyzer, with a repeatability of approximately 0.1 ppm (Zhou et al., 2005). The average time between sampling and analysis is about 2 months. All CO_2 measurements are also tied to the WMO CO_2 scale X2007. The co-located NOAA flask program at WLG ensures that the long-term CMA in -situ measurements can be routinely compared with an independent record.

Because of dead volumes in the in-situ sampling system, the response of the analyzer is usually not stable until 1 min after switching to a different gas source using the multi-position valve. Every standard gas cylinder was measured for 5 min and the data processing routine used the last 3 min of each 5 min segment to compute CO_2 mole fractions. The same is done for the ambient air data after switching in 5 min intervals from one sampling height to the other and after the reference gas measurements. The ambient measurements were calibrated using a linear two-point fit through the most recent standard gas measurements (WH & WL). Ambient CO_2 measurements were retained only during periods when the measurement of the most recent target gas (T) using this same calibration procedure was within ±0.1 ppm of its assigned value. Ambient air data were recorded as 5 min averages. More than 97 % of the total 5 min average data points were retained for meeting this criterion at the four stations.

After computing the CO_2 mole fractions, the data were manually inspected. Occasionally, analytical or sampling problems, including poor instrument performance or local influences such as nearby fires, vehicles, and cattle identified according to the station logbook entries made by the local operators affected the observations. Those events were eliminated prior to the next processing steps. More than 97 % of the 5 min data remained for each station after this filtering step. The 5 min data selected in that manner were then aggregated to hourly averages. To evaluate the seasonal cycle and

ACPD
13, 27287–27326, 2013

peak-to-peak amplitude, we used the curve fitting method described by Thoning et al. (1989). The data were first fitted to a function with 3 polynomial terms and 4 harmonic terms. Residuals from the function were then filtered (smoothed) in the time domain using two different low pass filters (Butterworth filter, which computes weighted averages over 1.07 yr at Full Width at Half Maximum of the weighting function, and the second filter 1.5 month at FWHM). The smoothed residuals are then added to the function to obtain smoothed time series with the seasonal cycle removed (1.07 yr FWHM) or representative of about monthly values for the second filter, as seen in Fig. 2. All of the averaged data in this study were reported with 95 % confidence intervals (CI).

3 Results and discussions

3.1 Carbon dioxide data

Fig. 2 shows the hourly averages of the processed ambient air CO_2 data at the 4 stations. The data gaps at WLG are due to a malfunction of the instrument. Valid flask sample pair measurements at WLG during the same period are also shown. To test the data quality of the Picarro system, differences between discrete flask measurements from NOAA ESRL and corresponding hourly CO_2 values from the Picarro instrument at WLG are studied. During most of time, differences between flasks and in-situ systems vary by ±1 ppm. The mean value of the difference (flask minus in-situ) is 0.1 ± 0.1 ppm (95 % CI, the same as below) for 168 sampling events (336 flasks). This result suggests that NOAA flask and CMA in-situ measurements at WLG are in good agreement and the CMA calibration and quality control procedures are well implemented without generating systematic biases. The differences between the two data sets are likely due to the sampling height and method (Zhou et al., 2005). The discrete flask sampler collects air 5 m above the ground while the in-situ system is measuring air at 80 m. Due to unique topography at WLG station (located at the top of mountain Waliguan in Tibetan plateau), the flask samples are collected at 08:00 (Local time) in the morning

ACPD
13, 27287–27326, 2013

before the updraft in the daytime may bring the local contaminations from the valley. The NOAA flask sampler collects air samples almost instantaneously (sampling period < 1 min) whereas the Picarro system generally has a continuous coverage during each hour. Thus, a part of the differences can be most likely explained by the atmospheric CO_2 fluctuations.

3.2 Mean diurnal cycles

The mean diurnal cycles of CO_2 variations in April, July, October, and January are used to represent the average variations in spring, summer, autumn, and winter. Only days containing 24 hourly average values are used, because the day-to-day variations of CO_2 can be quite large. The mean diurnal variations are shown in Fig. 3. Generally, diurnal variations of atmospheric CO_2 are affected by two factors: local sources/sinks and short/medium range transport (Artuso et al., 2009; Gerbig et al., 2006). In summer, the CO_2 diurnal variation has a similar phase between the sites, with peak value in the early morning and minima in afternoon. After sunrise, photosynthetic CO_2 uptake and mixing of near surface air with lower concentrations aloft makes the CO_2 mole fractions decrease gradually and reach a stable minimum at about 14:00–16:00 LT. In the late evening, when respiration dominates and the boundary layer becomes neutral or stable, CO_2 increases near the surface, and reaches a maximum at 06:00–07:00 LT in the morning, except at LFS where maximum values are observed at ~ 05:00 LT. The earlier maximum at LFS is likely due to an earlier sunrise time.

The LAN station is located in the subtropics. Compared with the other three stations, variations of air temperature (yearly average: 14 °C and solar radiation are relatively small during the year. As a result, photosynthetic/respiration fluxes are active (Kerang et al., 2004) in all seasons and diurnal CO_2 variations are thus significant throughout the year. The peak to peak mean diurnal amplitudes are 20.7 ± 5.0, 43.2 ± 6.4, 20.0 ± 4.0 and 8.3 ± 4.6 ppm for spring, summer, autumn and winter, respectively. The larger amplitude in summer is due to the higher temperature and solar radiation, which stimulate the assimilation in the daytime and respiration in the night.

ACPD
13, 27287–27326, 2013

Distinct CO_2 variations at LFS are also observed in summer. The diurnal amplitude is 50.6 ± 7.0 ppm, which is larger than at the other three stations. This is likely due to the active CO_2 fluxes from nearby paddy rice fields and forests (Yue et al., 2005). The LFS station is located in the most important rice production area ($> 40\,000\,km^2$) of China. In spring and autumn, the CO_2 diurnal variations are moderate, and display maxima in the morning and minima in the afternoon with a peak to peak amplitude of 4.5 ± 1.9 ppm in spring and 7.3 ± 4.8 ppm in autumn. There is no clear diurnal CO_2 variation in winter ($< 1.9 \pm 2.9$ ppm), which reflects weak local sources at LFS station.

The SDZ station exhibits complex CO_2 variations in the four seasons. In summer, the confidence intervals of the hourly averages (error bars in Fig. 3) are the highest among the four stations. The mean standard deviations for hourly CO_2 values are 9.5, 21.5, 15.9 and 12.7 ppm for spring, summer, autumn and winter, respectively which is much higher than for the other stations. These large values imply that the day to day variations of CO_2 are large compared to the periodic diurnal cycle. It can also be inferred that this site may be influenced by nearby emissions. In spring and autumn, the diurnal variations have amplitudes of 5.5 ± 3.7 and 8.8 ± 6.7 ppm, respectively. The larger diurnal variation in autumn may be due to the straw burning in the northern China plain (Cao et al., 2008; Li et al., 2008). In summer and winter, the standard deviations of the hourly averages are so large that the daily amplitudes could not be calculated.

The WLG high mountain station receives well-mixed air masses from the lower troposphere, with very small diurnal variability (see also Keeling et al., 1976). CO_2 are systematically lower than at the three regional near surface stations. Diurnal cycles are small throughout the year with largest intensity in summer when a diurnal amplitude of 3.4 ± 1.4 ppm is recorded. Observed seasonal and diurnal variations are similar to those observed from 1994 to 2000 reported by Zhou et al. (2002). Nevertheless, the smaller variations may also be partly due to the higher sampling intake height at WLG.

ACPD
13, 27287–27326, 2013

3.3 Comparison of CO_2 mole fractions between different levels

To understand the effect of local sources on observed CO_2 values, the hourly differences (over 1 yr record) between 10 m and the top of the sampling tower (50 m for LAN and 80 m for LFS) are shown in Fig. 4 (excepted for SDZ where the record is too short which only contains six months). Generally, CO_2 mole fractions at 10 m are higher than the top levels. The differences at LAN and LFS show distinct diurnal variations with large positive values at night (or early morning) and smaller values in the daytime, partly driven by the coupling between respired CO_2 emitted at night that usually accumulates in a shallow stable nocturnal boundary layer and net CO_2 uptake and efficient vertical mixing during daytime. At night, the maximum differences are 4.8 ± 0.5 ppm for LAN and 7.6 ± 1.3 ppm for LFS. The larger difference at LFS reflects there are stronger sources near the LFS observatory. Nevertheless, the height of top level at LAN (50 m) may also contribute to the smaller difference. In the midday, differences at the two regional stations are the smallest and relatively stable. The values are less than 0.2 ± 0.2 ppm from 10 to 16:00 LT at LAN and 0.3 ± 0.2 ppm from 09:00 to 16:00 LT at LFS. Given the CO_2 diurnal variations at the two regional stations, the observed data during these periods should be the least influenced by local sources. These significant differences between 10 m and 50/80 m due to the covariance of local vegetation fluxes with vertical mixing prevents inversion models to use night-time data at 10 m for regional flux estimates. Data during daytime at 10 m could be used in inversions with a bias correction of 0.2 to 0.3 ppm. The magnitude of this correction has to be compared with mean daytime CO_2 spatial gradients between stations, upon which are constrained inversion fluxes.

3.4 Impact of local surface wind

To understand the influence of local surface wind on the observed CO_2 results, average CO_2 during the whole observed period associated with different wind directions in the

ACPD
13, 27287–27326, 2013

Spring: March to May, Summer: June to August, Autumn: September to November, Winter: December to February are plotted in Figs. 5 to 8.

At LAN, in the four seasons, winds from the SW-SSW are associated with higher CO_2 mole fractions relative to the seasonal average (Fig. 5). Especially in autumn, the maximum enhancement relative to the seasonal average (407.5 ± 0.4 ppm) is 7.4 ± 1.6 ppm when winds are from SW sector. This direction is the town of Lin'an, 6 km away. The higher wind speed (average $> 1.6\,m\,s^{-1}$) in the four seasons (Fig. 5) may easily bring emissions from there. It is interesting to note that during the winter, the wind rose distribution pattern is different from the other seasons with higher CO_2 values on northeast direction. The maximum CO_2 is from the ENE sector, with values of 3.7 ± 1.7 ppm higher than the average seasonal value (413.9 ± 0.3 ppm). The higher values from the NE to E sectors are likely due to the transport of CO_2 emitted from Shanghai and Hangzhou cities (200 and 50 km from the station) whereas in the other seasons, vegetation uptakes atmospheric CO_2 and weakens the regional source strength signal during transport.

At LFS, in spring, summer and autumn, higher CO_2 is observed when winds are from the E to SSE sector (Fig. 6). A previous study also found that atmospheric CH_4 mole fraction in the SSE sector was much higher than in the other sectors (Fang et al., 2013). The LFS station is surrounded by forest and paddy rice fields, which are strong sinks for atmospheric CO_2. As a result, the lack of forests and paddy rice fields in the E to SSE sector (the Longfengshan reservoir is located in this sector) induces higher atmospheric CO_2 mole fractions. The maximum enhancement is 13 ± 3.2 ppm on E sector relative to the average value (389 ± 0.5 ppm) in summer. In winter, the average air temperature is lower than $-17\,^{\circ}C$. Emissions from the soil and plants are very weak and fossil fuel local emission (coal for domestic heating) is the main factor affecting the atmospheric CO_2 content. Because of the small villages to the north of LFS and the lower wind speed on this direction (Fig. 6), CO_2 in the WNW to N sector are higher with the largest value from the N sector, 3.6 ± 0.7 ppm above the average winter mean (404.6 ± 0.2 ppm).

ACPD
13, 27287–27326, 2013

The SDZ station is located in a complex terrain with many local and regional sources and sinks. The CO_2 distribution per wind sector differs in the four seasons (Fig. 7). The prevailing winds during the four seasons are ENE (> 10 %) and WSW (> 17 %). The wind speeds on these sectors are also higher than most sectors. Beijing is in the WSW direction. As a result, CO_2 on this sector is generally higher than from all other sectors. Especially in winter, CO_2 value is 11.7 ± 1.7 ppm higher from WSW than the seasonal mean (403.1 ± 0.4 ppm). A previous study of hydrofluorocarbons (HFCs) and perfluorocarbons (PFCs) at this station also observed that most compounds mole fractions are enhanced from WSW and SW directions (Yao et al., 2012). In addition, a railway (∼ 48 trains per day) running from south to north is at 600 m from the observatory. The higher CO_2 mole fractions from NW to SW sector all year round may also be partly due to emissions from diesel engine of the trains. When surface winds are from the mountain peak (north of the station), CO_2 mole fractions are obviously lower than the seasonal averages. The lowest decrease is in summer with a value of 6.4 ± 4.4 ppm lower than the seasonal average (402 ± 0.6 ppm). Obviously, surface winds originating from north may dilute the emissions in the valley and represent a better mixed volume in this area.

CO_2 mole fractions at WLG are relatively stable and have smaller variations in the four seasons. Similar to the analysis of CH_4 variability (Zhou et al., 2004), winds originating from NE-ENE sector are associated with CO_2 enhancements with a maximum value of 3.6 ± 1.0 ppm above the seasonal average (391.4 ± 0.1 ppm) in winter (Fig. 8). This likely reflects air masses exposed to regions with higher population density. Furthermore, Tang et al. (1999) studied the relationship of black carbon (BC) with surface winds and long-range transport and also found that the highest BC concentrations occur with air mass originating from the NE-NNE sector. They attributed these elevated BC concentrations to remote emissions from the Yellow River Canyon industrial area (including cities of Xining, Lanzhou etc.), 500 km to the northeast of WLG. This phenomenon is more obvious in winter when the absorption by the vegetation on the transporting path is very weak. The emissions from the capital of Qinghai Province

ACPD
13, 27287–27326, 2013

(Xining) (150 km to the northeast) are easily transported to the WLG and hence can cause elevated CO_2. In winter, in addition to NE-ENE sector, CO_2 values on E-ESE-SE sectors are also obviously higher. It is probably due to the emissions from coal burning for heating in Guide County, which is 5 km away east to the station.

Hourly CO_2 mole fractions during the three years were also calculated for different wind speeds (Beaufort scale): 0 scale: $<0.3\,m\,s^{-1}$, 1st scale: 0.3 to $1.5\,m\,s^{-1}$, 2nd scale: 1.6 to $3.3\,m\,s^{-1}$, 3rd scale: 3.4 to $5.4\,m\,s^{-1}$, 4th scale: 5.5 to $7.9\,m\,s^{-1}$, 5th scale: 8.0 to $10.7\,m\,s^{-1}$, 6th scale: 10.8 to $13.8\,m\,s^{-1}$, $\geq$ 7th scale: $\geq 13.9\,m\,s^{-1}$. Results show that the observed CO_2 value is strongly dependent on the wind speed at the four stations. At LAN, LFS and SDZ, lower CO_2 values are always accompanied with higher wind speed in the four seasons, even in summer when the local photosynthesis is very active. These results prove that higher wind speed (and longer range transport) may dilute the local emissions. Even in summer, the local anthropogenic emissions may be so strong that it plays a more important role than the biogenic sinks and sources. From the yearly average, the average CO_2 mole fractions are 416.2 ± 1.0, 402.7 ± 3.9 and 411.0 ± 1.3 ppm, respectively in calm conditions (scale-0). When the wind is on Beaufort scale 5, the average values are 397.1 ± 3.5, 397.2 ± 1.3 and 398.9 ± 1.4 ppm for LAN, LFS and SDZ, respectively. For WLG, in winter and spring, decreasing CO_2 values are also observed with increasing wind speed. However, during summer and autumn, an opposite behavior is observed. CO_2 increases with increasing wind speed, which may reflect that the local photosynthesis dilute the anthropogenic signals. For example, in summer, the average CO_2 mole fraction is 384.5 ± 1.5 ppm at calm condition (scale-0) and 388.2 ± 0.9 ppm on wind scale 7. The higher wind speed may bring emissions from a larger regional area (such as emissions from Northwest of China, Xining city of Qinghai province) and contribute to the higher CO_2 mole fractions.

The analysis of the diurnal patterns and the influence of different wind regimes on the observed CO_2 mole fractions at the three regional stations (LAN, LFS, and SDZ) reveal that the CO_2 levels are considerably driven by local anthropogenic and biogenic sources and sinks. In order to retrieve more regionally representative information on

ACPD
13, 27287–27326, 2013

the atmospheric CO_2 burden in China, in the following the data were split into two subsets.

3.5 Evaluation of "regional" mole fractions

A data filtering approach was applied to the CO_2 data at the three regional stations (SDZ, LFS and LAN), to divide the time series into periods under predominantly "local" and "regional" influence. Regional episodes rather represent CO_2 levels driven primarily by distant sources and sinks ($> \sim 10$ km), while the CO_2 mole fractions during local episodes are more strongly influenced by local sources and sinks ($\leq \sim 10$ km). Comparing measurements from the 10 m intake and the top level of the sampling tower show that during the midday when the boundary layer is high, atmospheric CO_2 mole fractions are the least influenced by local sources and the differences between the two levels are at a minimum. However, even during mid-day there is still a mixture of regional and local evens because the local sources and sinks are so strong at the regional stations. To get "the least influenced" CO_2 mole fractions, the local surface wind speed and wind rose distribution patterns are further used to flag the data.

Based on the analysis of the observed diurnal cycles and the comparison of the CO_2 mole fractions at the different inlet heights (Sects. 3.2 and 3.3), hourly data were considered to be regionally representative during daytime hours, i.e. from 09:00 LT to 17:00 LT at LAN and during 08:00 LT and 17:00 LT at LFS and SDZ. As discussed in Sect. 3.2, WLG is a remote measurement station with only small diurnal variations of atmospheric CO_2 mole fractions except in summer, when a systematic pattern is observed. Thus for WLG, only data from 06:00 to 07:00 LT in summer are considered to be under local influence when the observed CO_2 mole fractions are about 1.9 ± 0.8 ppm higher than the seasonal average (385.2 ± 0.1 ppm). All other data are treated as regionally representative.

Local meteorological conditions are then used to further filter the remaining data. Based on the discussion in Sect. 3.4, at low wind speeds, local emissions typically play a larger role on observed CO_2 mole fractions than at high wind speeds. Thus for LAN,

ACPD
13, 27287–27326, 2013

LFS and SDZ, CO_2 data are rejected when surface winds speeds are below 1.5 m s^{-1} (scale-0 & 1). At WLG, as discussed above, higher wind speeds may also transport emissions from the broader region and induce higher CO_2 mole fractions. Thus the CO_2 mole fractions are excluded to be regional when surface wind speeds are below 1 scale or over scale 6.

Finally, the CO_2 values are considered to be locally influenced when CO_2 mole fractions from a specific wind sector are higher than the corresponding seasonal means for all sectors. At LAN, these are SW sector for spring, SW to SSW and W to NNW sector for summer, S to WNW sector for autumn, and SW to S, SE, E to NE sector for winter (Fig. 5). At LFS, they are E to ESE and SSE sector for spring, E to SSE sector for summer and autumn, WNW to N sector for winter (Fig. 6). At SDZ, they are ENE to S, and WSW to W sector for spring, WNW to SSE sector for summer, SE, S, and SW to W sector for autumn, S to NW sector for winter (Fig. 7). At WLG, CO_2 data were split into "regional" and "local" according to the previous suggestion by Zhou et al. (2004). The locally influenced sectors there are NNE to NE sector for spring, NE to ENE, and SSW to NW sector for summer, NE to ENE sector for autumn, and NE to SE sector for winter (Fig. 8).

After the three steps filter, one subset for each station is considered to be minimally influenced by local sources, measured during so-called regional events. For the 3 regional stations, about 16.4 %, 24.7 % and 18.5 % of hourly CO_2 data are selected as regionally for LAN, LFS and SDZ, representatively. On the other hand, the large ratios of local events (possibly affected by local sources) prove that local sources strongly affect the CO_2 results at 10 m intakes. The regional events at WLG account for about 62.6 % of the total values, which reflects that the observations at WLG (at 80 m intake height) represent well-mixed air masses from the lower troposphere.

ACPD
13, 27287–27326, 2013

3.6 Long-term trends

The long-term trend of CO_2 is calculated using a linear fit to the regional data of the four stations. The regionally representative mole fractions at the four stations all show a positive trend in the last three years, of 2.2 ± 0.2, 2.3 ± 0.2, 2.0 ± 0.2 and 1.2 ± 0.1 (1σ) ppm yr^{-1} for LAN, LFS, SDZ and WLG, respectively. The increasing rates at the three regional stations (LAN, LFS and SDZ) are similar to the global values (2.3 ppm from 2009 to 2010, and 2.0 ppm from 2010 to 2011) (WMO greenhouse gas bulletin, 2011, 2012) and to the average of the past decade (~ 2.0 ppm yr^{-1}) (WMO, 2012). The increasing rate at WLG station should be underestimated because of the several data gaps during the observation period, especially the large data gap from 1 October to 30 December 2011, when high CO_2 mole fractions would be expected. During the same period, the CO_2 growth rate from the discrete flask samples analyzed by NOAA/ESRL is ~ 1.8 ppm yr^{-1}, which may be viewed as the growth rate at WLG station. The growth rates of the data influenced by local sources are 1.6 ± 0.1, 2.9 ± 0.1, 4.1 ± 0.2 and 1.3 ± 0.1 ppm yr^{-1} for LAN, LFS, SDZ and WLG, respectively. The increase rates of local events at LFS and SDZ are obviously higher than the global average, which may reflect that the sources in these areas increased during the last three years. Oppositely, at LAN station, the growth rate at local is a little bit smaller than regional value, which indicates the sources in this area might weaken in the last several years. Nevertheless, the differences from regional growth rates may also partly be ascribed to the different wind speed component at these stations.

3.7 Seasonal variations of regional CO_2 mole fractions

To evaluate the seasonal cycle and long-term trend in the regionally representative records, we use the curve fitting method described by Thoning et al. (1989) to get the CO_2 seasonal variations (Figs. 2 and 9). For comparison, we also overlay the simulated surface values at similar latitude to the four stations from the Marine Boundary Layer (MBL) reference computed by NOAA/GMD (LAN, sine of latitude value: 0.5, WLG, 0.6,

ACPD
13, 27287–27326, 2013

SDZ, 0.65, and LFS, 0.7) (Conway et al., 2013b). Seasonal cycle of CO_2 in the Northern Hemisphere is mainly dominated by exchange with the land biosphere and thus characterized by rapid decreases from June to August and large returns from September to December (Nevison et al., 2008; WMO, 2012). At the four stations, CO_2 minimum values all occur in August, which are similar with the Northern Hemisphere (MBL), and the occurring time at WLG consists with the previous study by Zhou et al. (2005). However, the seasonal CO_2 maximum occurring times vary a lot, ranging from January for LFS and LAN, March for SDZ to April for WLG. This difference is thought to be caused not only by regionally different terrestrial ecosystems and human activities but also by local meteorological conditions (Zhang et al., 2008). The high CO_2 mole fractions observed at LFS in winter is likely due to regional coal burning (heating) and biomass burning (agricultural fires) which begins in October in the northeastern China plain. LAN is located in the Yangtze Delta area, which is the most economically developed region in China. In winter, in addition to the lower boundary layer, the increase of fossil fuel consumption may also partly contribute to the higher CO_2 mole fractions. The maximum CO_2 mole fraction occurring time at WLG, a global WMO background site, agrees with the MBL and those observed at similar latitudes sites (Nakazawa et al., 1993; Riley et al., 2005; Throng et al., 1989).

At LAN, the monthly CO_2 mole fractions are obviously higher than the similar MBL (sine of latitude value: 0.5) references during the whole year with an average monthly difference of 11.2 ± 4.3 (1σ) ppm, which means the LAN area (Yangtze Delta area) is a very strong source of regional CO_2. Similarly, the CO_2 values at SDZ are also generally higher than the values at similar latitude (sine of latitude value: 0.65) with a mean of 6.2 ± 3.1 ppm (1σ). Both stations display larger difference with the MBL in the autumn and winter period and smaller values in summer. Because WLG is located at a high altitude and remote area, the observed values are close to the MBL references. The CO_2 values at LFS are strongly affected by local vegetation canopy in summer. As a result, CO_2 mole fractions are apparently lower than the MBL reference during the same period, with the maximum difference of -15.1 ± 5.8 ppm (1σ), which indicates

ACPD
13, 27287–27326, 2013

that the LFS area may act as a sink of background CO_2 in the summer. In the other seasons, similar to LAN and SDZ, CO_2 values are also obviously higher than the MBL references.

Table 2 illustrates the average regional CO_2 mole fractions and peak to peak amplitudes at the four sites. CO_2 mole fractions at WLG are generally lower than those observed at the three regional stations and the seasonal peak to peak amplitude is 10.4 ± 0.4 ppm, which is close to similar MBL value (~ 11.4 ppm, sine of latitude value: 0.6) and the previous study (10.5 ppm) by Zhou et al. (2005). The amplitudes from the three regional stations are obviously larger than WLG, which are mainly due to the strong sources and sinks in the regional areas. Because of the strong absorption by the rice plants and forest in the northeastern China plain, CO_2 mole fractions at LFS are extremely low in the summer and the peak to peak amplitude reaches to 37.3 ± 1.4 ppm, which is the highest among the four stations. The amplitude at LFS in this study is also much higher than that (19.3 ± 4.1 ppm) by Zhang et al. (2008) during 2003 to 2006. However, they used discrete flask sampling method, which might underestimate the value.

Table 3 illustrates the annual CO_2 values from the four stations. For comparison, we also present the values from Mauna Loa in United States (MLO) (Conway et al., 2013a), Jungfraujoch in Switzerland (JFJ), and Ryori in Japan (RYO) during the same period. MLO and JFJ are WMO/GAW global measurement stations. RYO is GAW regional measurement stations. The average regional CO_2 values at LAN, LFS and SDZ are obviously higher than the global mean value (~ 389 ppm in 2010 and 390.9 ± 0.1 ppm in 2011) (WMO greenhouse gas bulletin, 2011, 2012) and other WMO/GAW global stations such as MLO, JFJ. Compared with the results from other regional stations (such as RYO) close to China, CO_2 mole fractions at the three regional stations are also higher, proving that the stations in China are influenced by (domestic) CO_2 emissions. The highest annual mean CO_2 values are observed at LAN with a yearly value of 404.1 ± 4.1 ppm in 2011. It is because that there are megacities (Shanghai and Hangzhou) in this region and are also many industrial sources such as coal-fired power

ACPD
13, 27287–27326, 2013

plants (Wang et al., 2006; Zeng et al., 2008). Similar with methane (Fang et al., 2013), it also has a high level CO_2 mole fractions. The strong absorption by local vegetation obviously decreases the atmospheric CO_2 mole fractions at LFS. As a result, the annual mole fractions (Table 3) at this station are relatively lower than those at LAN and SDZ.

4 Conclusions

Atmospheric CO_2 measurements made at four WMO/GAW stations in China have been reported. The diurnal patterns, surface wind effects, atmospheric trends, and seasonal variations at each site were discussed. The results indicate that CO_2 mole fractions from 10 m above the ground at the three regional stations (LAN, LFS and SDZ) are more affected by local sources. Measurements from WLG are representative of the Tibetan Plateau.

The CO_2 mole fractions at the three regional stations are generally higher than the values at respective similar latitude from MBL references. CO_2 levels at LAN are representative of the Yangtze Delta area, China and are the highest among the four stations. Atmospheric CO_2 at LFS are strongly affected by local vegetation (paddy rice and forest) in summer. As a result, it has the lowest CO_2 levels in summer and the highest seasonal amplitude among the four stations. The SDZ station is located in an area with complex topography. The day to day variation of atmospheric CO_2 is quite large. CO_2 increases in case of events with local influence are highest at SDZ among the four stations. The seasonal CO_2 variations at WLG are small and similar with other GAW global stations (such as MLO in United States, and JFJ in Switzerland) with peak values occurring in spring.

In this study, we present continuous atmospheric CO_2 measurements from 2009 to 2011. The relatively short 3 yr record may introduce bias in our analysis of the seasonal variations and estimates of trends. However, the present analysis gives a first very valuable insight in the evolution and distribution of CO_2 mole fractions across China. To

ACPD
13, 27287–27326, 2013

better understand atmospheric CO_2 in China, a more extensive CO_2 observing network and longer period of in-situ measurements is required.

Acknowledgements. We express our great thanks to the staff at Lin'an, Longfengshan, Shangdianzi and Waliguan station who have contributed to the system installation and maintenance at the stations. This work is supported by National Natural Science Foundation of China (No. 41175116), the National Key Basic Research Program (No. 2010CB950601), the International S&T Cooperation Program of the MOST (No. 2011DFA21090), and the CMA operational fund (2012Y003). The data used in this study will be available for public within the China Meteorological Administration (CMA) policy.

M. Steinbacher acknowledges funding through the GAW Quality Assurance/Science Actitity Centre (QA/SAC) Switzerland supported by MeteoSwiss.

We thank NOAA ESRL, Japan Meteorological Agency (JMA), and University of Bern for providing monthly CO_2 data from Mauna Loa (Hawaii) in the United States, Ryori in Japan, and Jungfraujoch in Switzerland from 2009 to 2011. The monthly data are downloaded from World Data Centre for Greenhouse Gases (WDCGG).

Finally, we also greatly appreciate NOAA ESRL for long-term cooperation on the WLG flask air sampling program and NDIR in-situ measurement program and Ken Massarie for helping us on the data comparison.

References

Artuso, F., Chamard, P., Piacentino, S., Sferlazzo, D. M., Silvestri, L. D., Sarra, A. D., Meloni, D., and Monteleone, F.: Influence of transport and trends in amtospheric CO_2 at Lampedusa, Atmos. Environ., 43, 3044–3051, 2009.

Broquet, G., Chevallier, F., Bréon, F.-M., Kadygrov, N., Alemanno, M., Apadula, F., Hammer, S., Haszpra, L., Meinhardt, F., Morguí, J. A., Necki, J., Piacentino, S., Ramonet, M., Schmidt, M., Thompson, R. L., Vermeulen, A. T., Yver, C., and Ciais, P.: Regional inversion of CO_2 ecosystem fluxes from atmospheric measurements: reliability of the uncertainty estimates, Atmos. Chem. Phys., 13, 9039–9056, doi:10.5194/acp-13-9039-2013, 2013.

Ballantyne, A. P., Alden, C. B., Miller, J. B., Tans, P. P., and White, J. W. C.: Increase in observed net carbon dioxide uptake by land and oceans during the past 50 years, Nature, 488, 70–73, 2012.

ACPD

13, 27287–27326, 2013

Cao, G., Zhang, X., Wang, Y., and Zheng, F.: Estimation of emissions from field burning of crop straw in China, Chinese Sci. Bull., 53, 784–790, 2008.

Chen, H., Winderlich, J., Gerbig, C., Hoefer, A., Rella, C. W., Crosson, E. R., Van Pelt, A. D., Steinbach, J., Kolle, O., Beck, V., Daube, B. C., Gottlieb, E. W., Chow, V. Y., Santoni, G. W., and Wofsy, S. C.: High-accuracy continuous airborne measurements of greenhouse gases (CO_2 and CH_4) using the cavity ring-down spectroscopy (CRDS) technique, Atmos. Meas. Tech., 3, 375–386, doi:10.5194/amt-3-375-2010, 2010.

Chevallier, F., Deutscher, N. M., Conway, T. J., Ciais, P., Ciattaglia, L., Dohe, S., Fröhlich, M., Gomez-Pelaez, A. J., Griffith, D., Hase, F., Haszpra, L., Krummel, P., Kyrö, E., Labuschagne, C., Langenfelds, R., Machida, T., Maignan, F., Matsueda, H., Morino, I., Notholt, J., Ramonet, M., Sawa, Y., Schmidt, M., Sherlock, V., Steele, P., Strong, K., Sussmann, R., Wennberg, P., Wofsy, S., Worthy, D., Wunch, D., and Zimnoch, M.: Global CO_2 fluxes inferred from surface air-sample measurements and from TCCON retrievals of the CO_2 total column, Geophys. Res. Lett., 38, L24810, doi:10.1029/2011GL049899, 2011.

Conway, T. J., Lang, P. M., and Masarie, K. A.: Atmospheric Carbon Dioxide Dry Air Mole Fractions from the NOAA ESRL Carbon Cycle Cooperative Global Air Sampling Network, 1968–2011, Version: 2012-08-15, ftp://ftp.cmdl.noaa.gov/ccg/co2/flask/event/ (last access: 28 August 2013), 2012a.

Conway, T. J., Masarie, K. A., Lang, P. M., and Tans, P. P.: NOAA greenhouse gas reference from atmospheric carbon dioxide dry air mole fractions from the NOAA ESRL Carbon Cycle Cooperative Global Air Sampling Network, (ftp://ftp.cmdl.noaa.gov/ccg/co2/flask/) (last access: 28 August 2013), 2012b.

Crosson, E. R.: A cavity ring-down analyzer for measuring atmospheric levels of methane, carbon dioxide, and water vapor, Appl. Phys. B, 92, 403–408, 2008.

Dlugokencky, E. J., Steele, L. P., Lang, P. M., and Masarie, K. A.: The growth rate and distribution of atmospheric methane, J. Geophys. Res., 99, 17021–17043, 1994.

Dlugokencky, E. J., Steele, L. P., Lang, P. M., and Masarie, K. A.: Atmospheric CH_4 at Mauna Loa and Barrow Observatories: presentation and analysis of in in situ measurements, J. Geophys. Res., 100, 23103–23113, 1995.

Fang, S. X., Zhou, L. X., Masarie, K. A., Xu, L., and Rella, C. W.: Study of atmospheric CH_4 mole fractions at three WMO/GAW stations in China, J. Geophys. Res., 118, 4874–4886, doi:10.1002/jgrd.50284, 2013.

ACPD
13, 27287–27326, 2013

Fu, Y., Zheng, Z., Yu, G., Hu, Z., Sun, X., Shi, P., Wang, Y., and Zhao, X.: Environmental influences on carbon dioxide fluxes over three grassland ecosystems in China, Biogeosciences, 6, 2879–2893, doi:10.5194/bg-6-2879-2009, 2009.

GLOBALVIEW-CO_2, Cooperative Atmospheric Data Integration Project – Carbon Dioxide. NOAA ESRL, Boulder, Colorado [Available at http://www.esrl.noaa.gov/gmd/ccgg/globalview/] (last access: 3 January 2013), 2012.

Gerbig, C., Lin, J. C., Munger, J. W., and Wofsy, S. C.: What can tracer observations in the continental boundary layer tell us about surface-atmosphere fluxes?, Atmos. Chem. Phys., 6, 539–554, doi:10.5194/acp-6-539-2006, 2006.

Gourdji, S. M., Mueller, K. L., Yadav, V., Huntzinger, D. N., Andrews, A. E., Trudeau, M., Petron, G., Nehrkorn, T., Eluszkiewicz, J., Henderson, J., Wen, D., Lin, J., Fischer, M., Sweeney, C., and Michalak, A. M.: North American CO_2 exchange: inter-comparison of modeled estimates with results from a fine-scale atmospheric inversion, Biogeosciences, 9, 457–475, doi:10.5194/bg-9-457-2012, 2012.

Houghton, R. A.: Revised estimates of the annual net flux of carbon to the atmosphere from changes in land use and land management 1850–2000, Tellus, 55, 378–390, 2003.

IPCC (Intergovernmental Panel on Climate Change): Climate Change 2007: The Physical Science Basis, Contribution of Working Group I to the Fourth Assessment, Report of the Intergovernmental Panel on Climate Change, edited by: Solomon, S., Qin, D., Manning, M., Chen, Z., Marquis, M., Averyt, K. B., Tignor, M., and Miller, H. L., Cambridge Univ. Press, New York, 2007.

Keeling, C. D.: Global observations of atmospheric CO_2, in: The Global Carbon Cycle, NATO ASI Series, vol. 15, edited by: Heimann, M., Springer-Verlag, New York, 1–30, 1993.

Keeling, C. D., Bacastow, R. B., Bainbridge, A., Ekdahl Jr., C. A., Guenther, P. R., Waterman, L. S., and Chin, J. F.: Atmospheric carbon dioxide variations at Mauna Loa Observatory, Hawaii, Tellus, 28, 538–551, 1976.

Keeling, R. F.: Recording earth's vital signs, Science, 319, 1771–1772, 2008.

Kerang, L., Wang, S., and Cao, M.: Vegetation and soil carbon storage in China, Sci. China, Ser. D , 47, 49–57, 2004.

Le Quéré, C., Andres, R. J., Boden, T., Conway, T., Houghton, R. A., House, J. I., Marland, G., Peters, G. P., van der Werf, G. R., Ahlström, A., Andrew, R. M., Bopp, L., Canadell, J. G., Ciais, P., Doney, S. C., Enright, C., Friedlingstein, P., Huntingford, C., Jain, A. K., Jourdain, C., Kato, E., Keeling, R. F., Klein Goldewijk, K., Levis, S., Levy, P., Lomas, M., Poulter, B.,

ACPD
13, 27287–27326, 2013

Raupach, M. R., Schwinger, J., Sitch, S., Stocker, B. D., Viovy, N., Zaehle, S., and Zeng, N.: The global carbon budget 1959–2011, Earth Syst. Sci. Data, 5, 165–185, doi:10.5194/essd-5-165-2013, 2013.

Lei, H. M. and Yang, D. W.: Seasonal and interannual variations in carbon dioxide exchange over a cropland in the North China Plain, Glob. Change Biol., 16, 2944–2957, 2010.

Liu, L., Zhou, L., Zhang, X., Wen, M., Zhang, F., Yao, B., and Fang, S., The characteristics of atmospheric CO_2 concentration variation of the four national background stations, China, Sci. China, Ser. D, 52, 1857–1863, 2009.

Li, L., Wang, Y., Zhang, Q., Li, J., Yang, X., and Jin, J.: Wheat straw burning and its associated impacts on Beijing air quality, Sci. China Ser. D, 51, 403–414, 2008.

Marland, G.: Emissions accounting: China's uncertain CO_2 emissions, Nat. Clim. Chang., 2, 645–646, 2012.

Nakazawa, T., Morimoto, S., Aoki, S., and Tanaka, M.: Time and space variations of the carbon isotopic ratio of tropospheric carbon dioxide over Japan, Tellus, 45, 258–274, 1993.

Necki, J., Schmidt, M., Rozanski, K., Zimnoch, M., Korus, A., Lasa, J., Graul, R., and Levin, I.: Six-year record of atmospheric carbon dioxide and methane at a high-altitude mountain site in Poland, Tellus, 55, 94–104, 2003.

Nevison, C. D., Mahowald, N. M., Doney, S. C., Lima, I. D., van der Werf, G. R., Randerson, J. T., Baker, D. F., Kasibhatla, P., and McKinley, G. A.: Contribution of ocean, fossil fuel, land biosphere, and biomass burning carbon fluxes to seasonal and interannual variability in atmospheric CO_2, J. Geophys. Res., 113, G01010, doi:10.1029/2007JG000408, 2008.

Peylin, P., Law, R. M., Gurney, K. R., Chevallier, F., Jacobson, A. R., Maki, T., Niwa, Y., Patra, P. K., Peters, W., Rayner, P. J., Rödenbeck, C., and Zhang, X.: Global atmospheric carbon budget: results from an ensemble of atmospheric CO_2 inversions, Biogeosciences Discuss., 10, 5301–5360, doi:10.5194/bgd-10-5301-2013, 2013.

Peters, G. P., Minx, J. C., Weber, C. L., and Edenhofer, O.: Growth in emission transfers via international trade from 1990 to 2008, Proc. Natl. Acad. Sci. USA, 108, 8903–3908, 2011.

Peters, G. P., Marland, G., Le Quéré, C., Boden, T., Canadell, J. G., and Raupach, M. R.: Rapid growth in CO_2 emissions after the 2008–2009 global financial crisis, Nat. Clim. Chang., 2, 2–4, 2012.

Peters, W., Jacobson, A. R., Sweeney, C., Andrews, A. E., Conway, T. J., Masarie, K., Miller, J. B., Bruhwiler, L. M. P., Pétron, G., Hirsch, A. I., Worthy, D. E. J., van der Werf, G. R., Randerson, J. T., Wennberg, P. O., Krol, M. C., and Tans, P. P.: An atmospheric perspective

ACPD
13, 27287–27326, 2013

on North American carbon dioxide exchange: CarbonTracker, Proc. Natl. Acad. Sci. USA, 104, 18925–18930, doi:10.1073/pnas.0708986104, 2007.
Riley, W. J., Randerson, J. T., Foster, P. N., and Lueker, T. J.: Influence of terrestrial ecosystems and topography on coastal CO_2 measurements: A case study at Trinidad Head, California, J. Geophys. Res., 110, G01005, doi:10.1029/2004JG000007, 2005.
Sirignano, C., Neubert, R. E. M., Rödenbeck, C., and Meijer, H. A. J.: Atmospheric oxygen and carbon dioxide observations from two European coastal stations 2000–2005: continental influence, trend changes and APO climatology, Atmos. Chem. Phys., 10, 1599–1615, doi:10.5194/acp-10-1599-2010, 2010.
Tang, J., Wen, Y. P., and Zhou, L. X.: Observational study of black carbon aerosol in western China, J. Appl. Meteor. Sci., 10, 160–170, 1999.
Tang, X., Liu, S., Zhou, G., Zhang, D., and Zhou, C.: Soil-atmospheric exchange of CO_2, CH_4 and N_2O in three subtropical forest ecosystems in southern China, Glob. Change Biol., 12, 546–560, 2006.
Tans, P. P., Fung, I. Y., and Takahashi, T.: Observation constraints on the global atmospheric CO_2 budget, Science, 247, 1431–1438, 1990.
Thompson, R. L., Manning, A. C., Gloor, E., Schultz, U., Seifert, T., Hänsel, F., Jordan, A., and Heimann, M.: In-situ measurements of oxygen, carbon monoxide and greenhouse gases from Ochsenkopf tall tower in Germany, Atmos. Meas. Tech., 2, 573–591, doi:10.5194/amt-2-573-2009, 2009
Thoning, K. W., Tans, P. P., and Komhyr, W. D.: Atmoshperic carbon dioxide at Mauna Loa observatory 2. Analysis of the NOAA GMCC data, 1974–1985, J. Geophys. Res., 94, 8549–5865, 1989.
Wang, H., Zhou, L., and Tang, X.: Ozone concentrations in Rural Regions of the Yangtze Delta in China, J. Atmos. Chem., 54, 266–265, 2006.
World meteorological organization (WMO): WMO World Data Centre for Greenhouse Gases (WDCGG) Data Summary: Volume IV – Greenhouse Gases and Other Atmospheric Gases, No. 36, Japan Meteorological Agency, http://ds.data.jma.go.jp/gmd/wdcgg/products/summary/sum36/sum36contents.html (last access: 1 March 2012), 2012.
Xing, Y., Xie, P., Yang, H., Ni, L., Wang, Y., and Rong, K.: Methane and carbon dioxide fluxes from a shallow hypereutrophic subtropical lake in China, Atmos. Environ., 39, 5532–5540, 2005.

ACPD
13, 27287–27326, 2013

WMO greenhouse gas bulletin: The state of greenhouse gases in the atmosphere based on global observations through 2010. Geneva: World Meteorological Organization, 2011.
WMO Greenhouse Gas Bulletin: The state of greenhouse gases in the atmosphere based on global observations through 2011, Geneva: World Meteorological Organization, 2012.
Yao, B., Vollmer, M. K., Zhou, L. X., Henne, S., Reimann, S., Li, P. C., Wenger, A., and Hill, M.: In-situ measurements of atmospheric hydrofluorocarbons (HFCs) and perfluorocarbons (PFCs) at the Shangdianzi regional background station, China, Atmos. Chem. Phys., 12, 10181–10193, doi:10.5194/acp-12-10181-2012, 2012.
Yue, J., Shi, Y., Liang, W., Wu, J., Wang, C., and Huang, G.: Methane and nitrous oxide emissions from rice field and related microorganism in black soil, northeastern China, Nutr. Cycl. Agroecosys., 73, 293–301, 2005.
Zeng, N., Ding, Y., Pan, J., Wang, H., and Gregg, J.: Climate Change – the Chinese Challenge, Science, 319, 730–731, 2008.
Zhang, D., Tang, J., Shi, G., Nakazawa, T., Aoki, S., Sugawara, S., Wen, M., Morimoto, S., Patra, P. K., and Hayasaka, T.: Temporal and spatial variations of the atmospheric CO_2 concentration in China, Geophys. Res. Lett., 35, L03801, doi:10.1029/2007GL032531, 2008.
Zhao, C. L. and Tans, P. P.: Estimating uncertainty of the WMO mole fraction scale for carbon dioxide in air, J. Geophys. Res., 111, D08S09, doi:10.1029/2005JD006003, 2006.
Zhao, C., Tans, P. P., and Thoning, K. W.: A high precision manometric system for absolute calibrations of CO_2 in dry air, J. Geophys. Res., 102, 5885–5894, 1997.
Zhou, L., Conway, J. T. J., White, W. C., Mukai, H., Zhang, X., Wen, Y., Li, J., and MacClune, K.: Long-term record of atmospheric CO_2 and stable isotopic ratios at Waliguan Observatory: Background features and possible drivers, 1991–2002, Global Biogeochem. Cy., 19, GB2001, doi:10.1029/2004GB002430, 2005.
Zhou, L. X., Worthy, D. E. J., Lang, P. M., Ernst, M. K., Zhang, X. C., Wen, Y. P., and Li, J. L.: Ten years of atmospheric methane observations at a high elevation site in Western China, Atmos. Environ., 38, 7041–7054, 2004.
Zhou, L. X., Tang, J., Wen, Y. P., Li, J. L., Yan, P., and Zhang, X. C.: The impact of local winds and long-range transport on the continuous carbon dioxide record at Mount Waliguan, China, Tellus, 55, 145–158, 2003.
Zhou, L., Tang, J., Wen, Y., Zhang, X., and Nie, H.: Impact of local surface wind on the atmospheric carbon dioxide background concentration at Mt. Waliguan, Acta Scientiae Circumstantiae, 22, 135–139, 2002 (in Chinese).

ACPD
13, 27287–27326, 2013

Zhou, L. X., White, J. W. C., Conway, T. J., Mukai, H., MacClune, K., Zhang, X., Wen, Y., and Li, J.: Long-term record of atmospheric CO_2 and stable isotopic ratios at Waliguan Observatory: Seasonally averaged 1991–2002 source/sink signals, and a comparison of 1998–2008 record to the 11 selected sites in the Northern Hemisphere, Global Biogeochem. Cy., 20, GB2001, doi:10.1029/2004GB002431, 2006.

ACPD
13, 27287–27326, 2013

Table 1. Descriptions of the four WMO/GAW stations in China.

Station	Station ID	Longitude	Latitude	Altitude (m a.s.l.)	Intake height (m a.g.l.)	Representation area	Vegetation canopy
Lin'an	LAN	119.73° E	30.3° N	138.6	10, 50	Chang River Delta Ecnomic Zone	Paddy, wheat field. Shrub
Longfengshan	LFS	127.6° E	44.73° N	330.5	10, 80	Northeastern Plain	Paddy, forest
Shangdianzi	SDZ	117.12° E	40.65° N	293.3	10, 80	The North China Plain	Corn, shrub
Mt. Waliguan	WLG	100.06° E	36.12° N	3816	10, 80	Northeastern of the Tibetan Plateau	Prairie, Sandbank

ACPD
13, 27287–27326, 2013

Table 2. Seasonal average mole fractions and amplitude of CO_2 from the "regional" data sets.

Season	LAN (ppm)	LFS (ppm)	SDZ (ppm)	WLG (ppm)
Spring (Mar–May)	403.3 ± 0.4	399.8 ± 0.2	399.4 ± 0.4	393.1 ± 0.1
Summer (Jun–Aug)	392.7 ± 0.6	374.4 ± 0.6	387.4 ± 0.6	384.5 ± 0.2
Autumn (Sep–Nov)	397.7 ± 0.6	394.8 ± 0.5	395.9 ± 0.6	388.5 ± 0.1
Winter (Dec–Next Feb)	407.0 ± 0.6	403.5 ± 0.3	398.4 ± 0.4	390.9 ± 0.1
Peak to peak amplitude	18.8 ± 1.8	37.3 ± 1.4	19.0 ± 1.9	10.4 ± 0.4

ACPD
13, 27287–27326, 2013

Table 3. Comparison of yearly CO_2 mole fractions with other WMO/GAW stations.

Station	Year	LAN	LFS	SDZ	WLG	RYO	MLO	JFJ
Latitude		30.18° N	44.73° N	40.65° N	36.3° N	39.03° N	19.54° N	46.55° N
Longitude		119.44° E	127.6° E	117.12° E	100.9° E	141.82° E	155.58° W	7.99° E
Altitude (m a.s.l.)		139	331	293	3816	260	3397	3580
Annual mean (ppm)	2009	397.2 ± 3.3	390.1 ± 7.0	392.3 ± 3.8	387.2 ± 2.1	389.8 ± 2.9	387.4 ± 1.1	388.2 ± 2.1
Annual mean (ppm)	2010	400.3 ± 4.2	393.8 ± 6.7	396.2 ± 3.4	389.5 ± 1.9	393.5 ± 2.1	389.8 ± 1.2	390.7 ± 2.1
Annual mean (ppm)	2011	404.1 ± 4.1	395.0 ± 7.4	397.2 ± 3.4	–	394.3 ± 2.8	391.6 ± 1.0	392.2 ± 2.0

"–": the years containing less than 12-month data are not calculated.

ACPD
13, 27287–27326, 2013

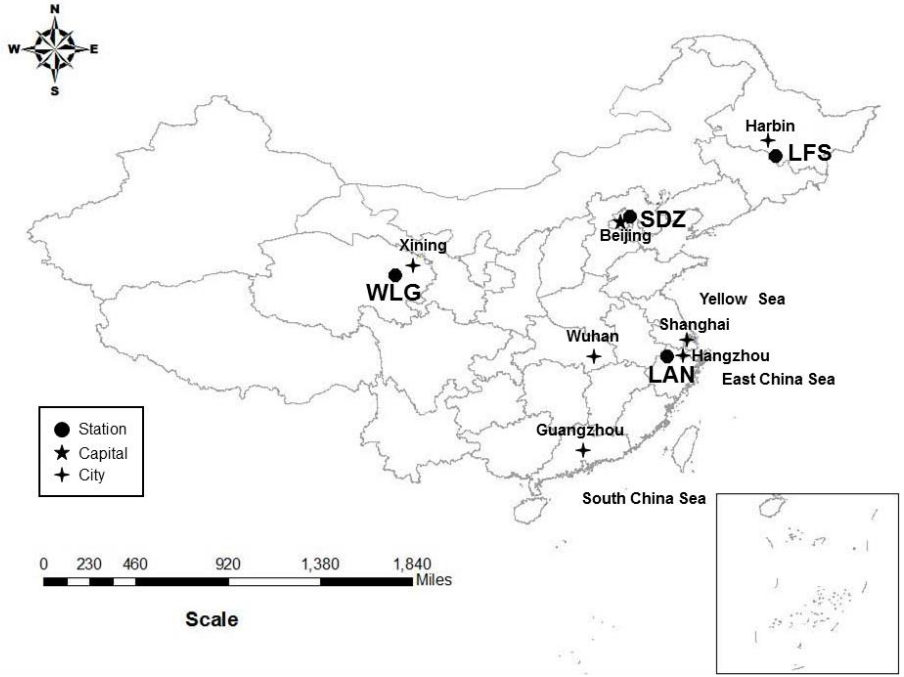

Fig. 1. Locations of the four WMO/GAW stations.

ACPD
13, 27287–27326, 2013

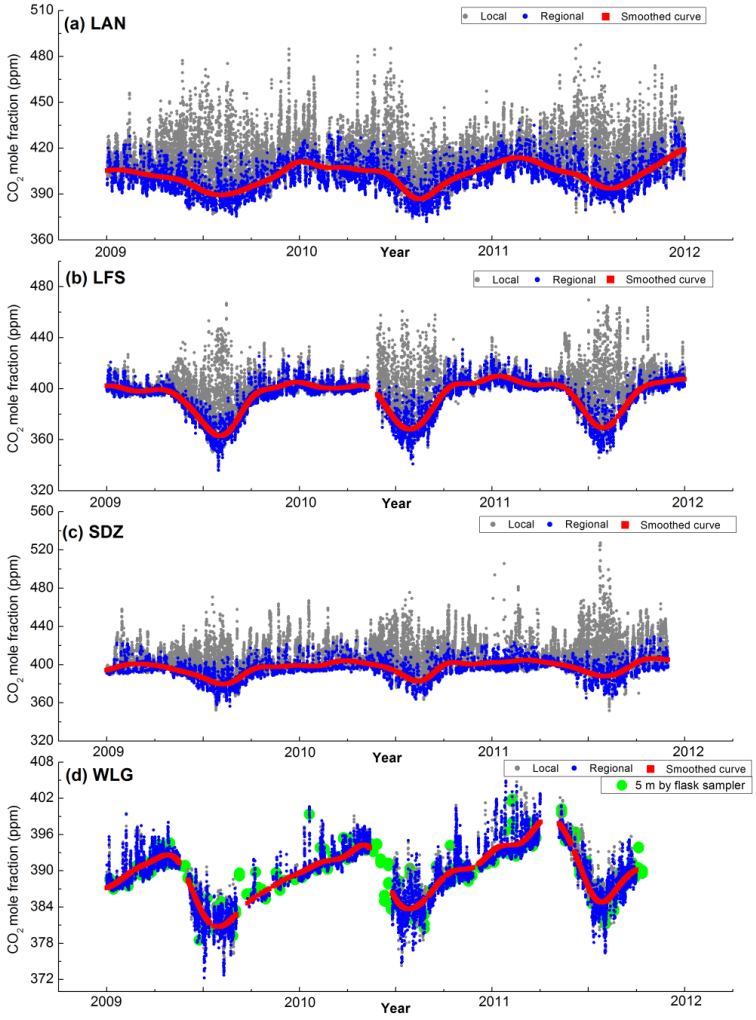

ACPD
13, 27287–27326, 2013

In-situ measurement of atmospheric CO_2 at the four WMO/GAW stations in China

S. X. Fang et al.

Fig. 2. Seasonal variations of hourly CO_2 mole fractions at **(a)** Lin'an (LAN), **(b)** Longfengshan (LFS), **(c)** Shangdianzi (SDZ), and **(d)** Mt. Waliguan (WLG). Grey dots are locally representative CO_2 mole fractions and the blue dots are regional records. See text for details. The red dots are curve fitted results to the regional records using the method by Thoning et al. (1989). The results at LAN, LFS and SDZ are from 10 m above the ground (a.g.l.). At WLG station **(d)**, grey and blue dots are values from 80 m a.g.l., and green dots denote discrete CO_2 flask pair measurement from the NOAA ESRL flask air-sampling program.

ACPD
13, 27287–27326, 2013

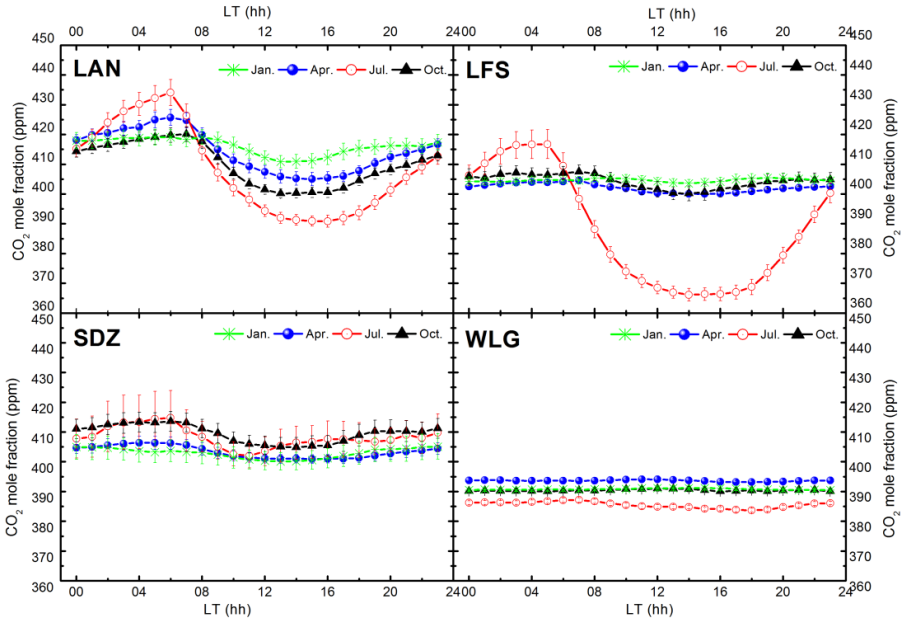

Fig. 3. Mean diurnal variations of CO_2 mole fractions in January, April, July and October. Error bars indicate confidence intervals of 95 %. LAN, LFS, and SDZ data are sampled at 10 m while WLG data are sampled at 80 m above ground.

ACPD
13, 27287–27326, 2013

In-situ measurement of atmospheric CO_2 at the four WMO/GAW stations in China

S. X. Fang et al.

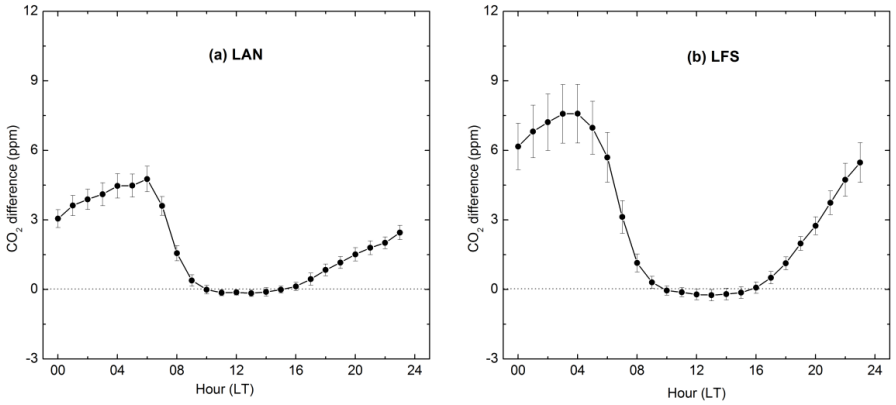

Fig. 4. Diurnal differences of hourly CO_2 mole fractions between the 10 m and the top of each tower (50/80 m) at the two regional stations. **(a)** LAN station, 10 m results minus 50 m values. **(b)** LFS station, 10 m results minus 80 m values. Error bars indicate confidence intervals of 95%.

ACPD
13, 27287–27326, 2013

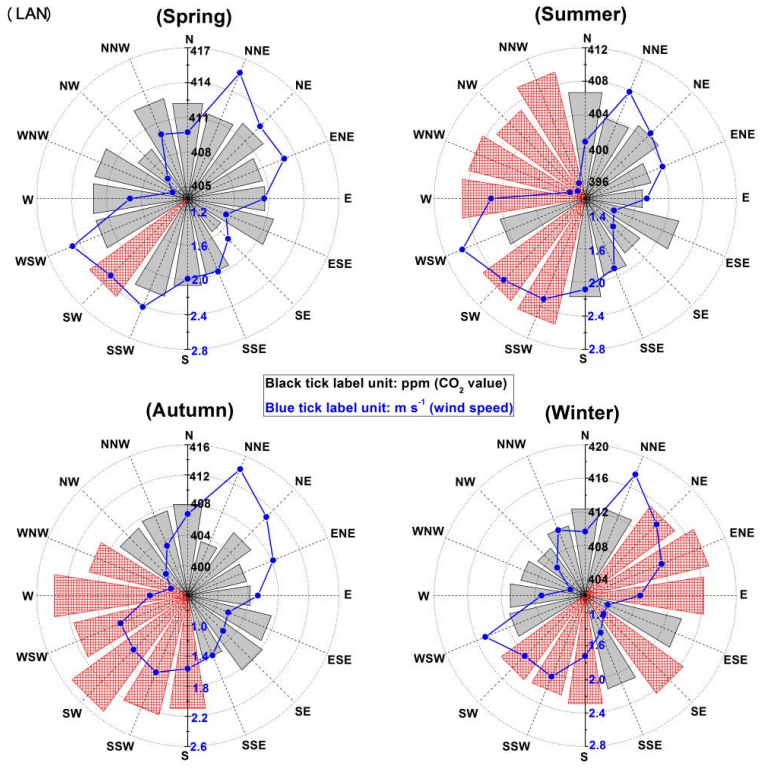

Fig. 5. Seasonal hourly CO_2 mole fractions and average wind speeds on the 16 horizontal wind directions at LAN. The light gray bars illustrate CO_2 mole fractions from wind sectors considered to be regionally representative while the red cross-line bars denotes data which are likely to be influenced by local sources. The blue dots and lines are average wind speeds.

ACPD
13, 27287–27326, 2013

In-situ measurement of atmospheric CO_2 at the four WMO/GAW stations in China

S. X. Fang et al.

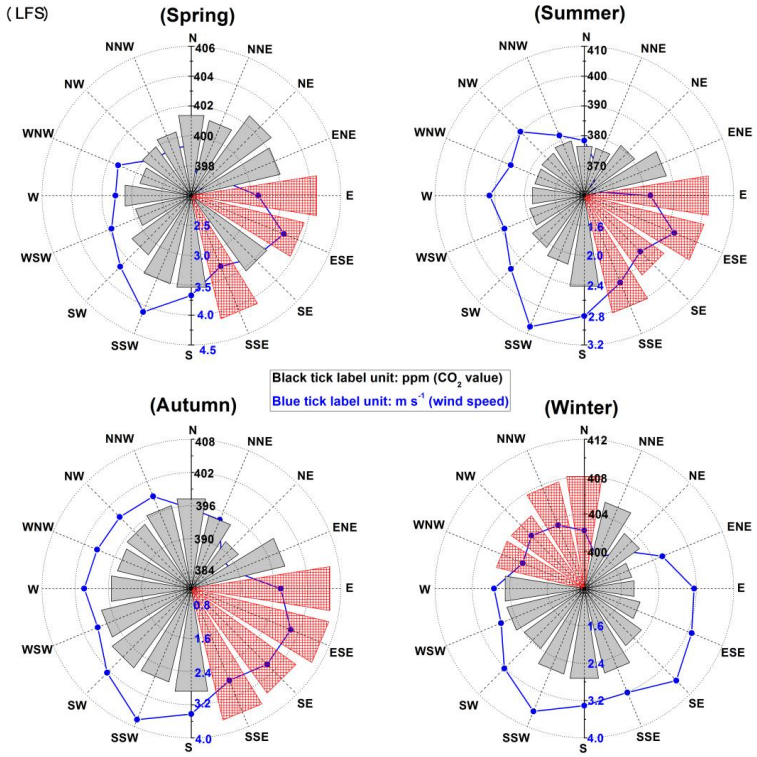

Fig. 6. Seasonal hourly CO_2 mole fractions and average wind speeds on the 16 horizontal wind directions at LFS. The light gray bars illustrate CO_2 mole fractions from wind sectors considered to be regionally representative while the red cross-line bars denotes data which are likely to be influenced by local sources. The blue dots and lines are average wind speeds.

ACPD
13, 27287–27326, 2013

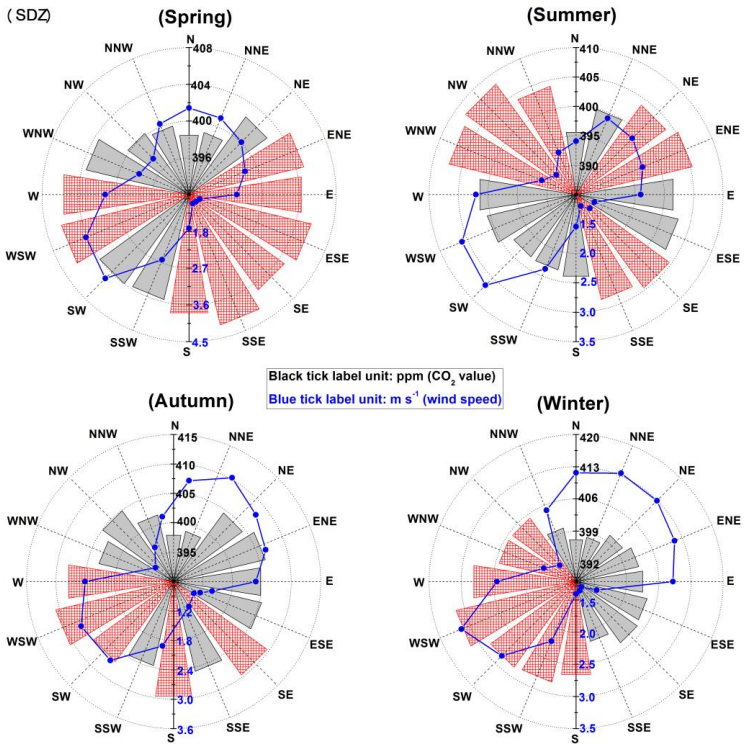

Fig. 7. Seasonal hourly CO_2 mole fractions and average wind speeds on the 16 horizontal wind directions at SDZ. The light gray bars illustrate CO_2 mole fractions from wind sectors considered to be regionally representative while the red cross-line bars denotes data which are likely to be influenced by local sources. The blue dots and lines are average wind speeds.

ACPD
13, 27287–27326, 2013

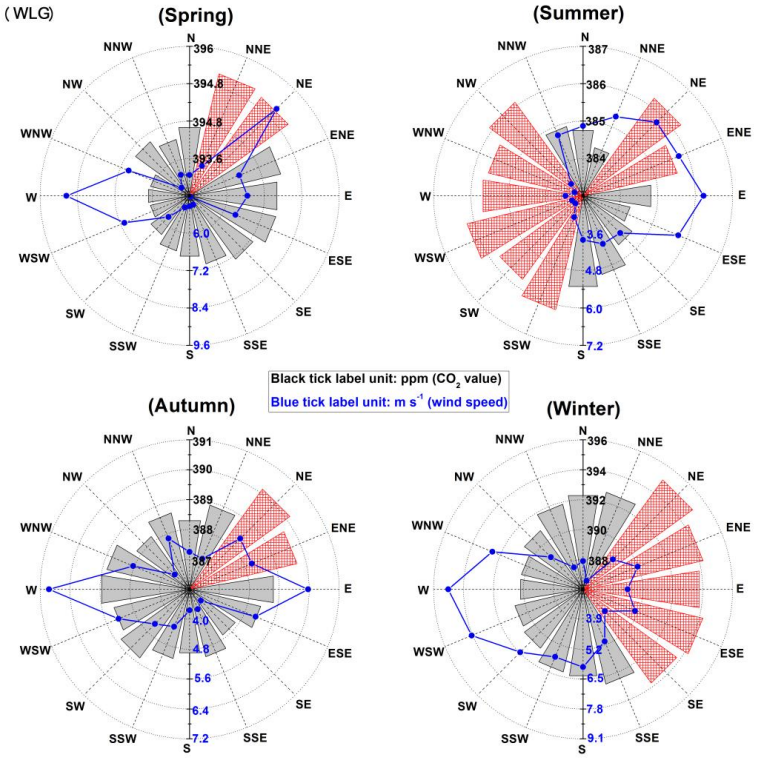

Fig. 8. Seasonal hourly CO_2 mole fractions and average wind speeds on the 16 horizontal wind directions at WLG. The light gray bars illustrate CO_2 mole fractions from wind sectors considered to be regionally representative while the red cross-line bars denotes data which are likely to be influenced by local sources. The blue dots and lines are average wind speeds.

ACPD
13, 27287–27326, 2013

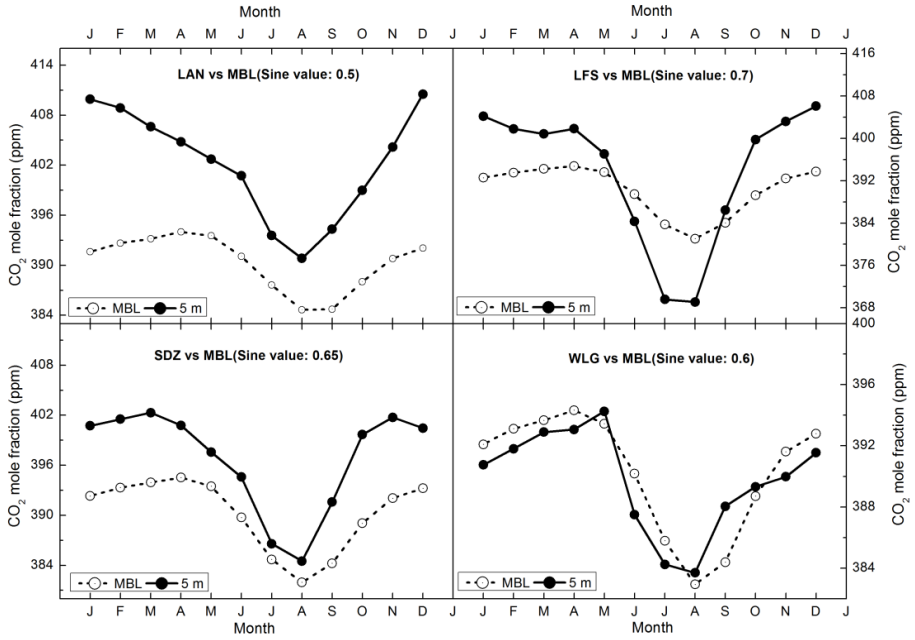

Fig. 9. Variations of monthly CO_2 mole fractions at LAN, LFS, SDZ and WLG during 2009 to 2011. Also compare to the surface values at similar latitudes from MBL reference (Conway et al., 2013b). LAN compares to those of sine of latitude value 0.5, WLG with 0.6, SDZ with 0.65 and LFS with 0.7. The close circles and solid line denote the monthly averaged values at the four stations. The open circles and dash lines denote the monthly average CO_2 values from MBL reference. The data in this figure are smoothed values from the curve fitting method by Thoning et al. (1989).

ACPD
13, 27287–27326, 2013

In-situ measurement of atmospheric CO_2 at the four WMO/GAW stations in China

S. X. Fang et al.